SCIENCE CHINA
Earth Sciences

• RESEARCH PAPER •

May 2012 Vol.55 No.5: 770–778
doi: 10.1007/s11430-012-4375-6

Analysis of reconstructed annual precipitation from tree-rings for the past 500 years in the middle Qilian Mountain

TIAN QinHua[1,2,3], ZHOU XiuJi[3*], GOU XiaoHua[2], ZHAO Ping[4], FAN ZeXin[5] & Samuli HELAMA[6]

[1] *National Climate Center, Beijing 100081, China;*
[2] *Center for Arid Environment and Paleoclimate Research (CAEP), Key Laboratory of Western China's Environment Systems MOE, Lanzhou University, Lanzhou 730000, China;*
[3] *Chinese Academy of Meteorological Sciences, Beijing 100081, China;*
[4] *National Meteorological Information Center, Beijing 100081, China;*
[5] *Xishuangbanna Tropical Botanical Garden, Chinese Academy of Sciences, Kunming 650223, China;*
[6] *Arctic Centre, University of Lapland, Rovaniemi 96101, Finland*

Received August 5, 2011; accepted October 29, 2011; published online March 30, 2012

The ring-width chronology of a *Juniperus przewalskii* tree from the middle of the Qilian Mountain was constructed to estimate the annual precipitation (from previous August to current July) since AD 1480. The reconstruction showed four major alternations of drying and wetting over the past 521 years. The rainy 16th century was followed by persistent drought in the 17th century. Moreover, relatively wet conditions persisted from the 18th to the beginning of 20th century until the recurrence of a drought during the 1920s and 1930s. Based on the Empirical Mode Decomposition method, eight Intrinsic Mode Functions (IMFs) were extracted, each representing unique fluctuations of the reconstructed precipitation in the time-frequency domain. The high amplitudes of IMFs on different timescales were often consistent with the high amount of precipitation, and *vice versa*. The IMF of the lowest frequency indicated that the precipitation has undergone a slow increasing trend over the past 521 years. The 2–3 year and 5–8 year time-scales reflected the characteristics of inter-annual variability in precipitation relevant to regional atmospheric circulation and the El Niño-Southern Oscillation (ENSO), respectively. The 10–13 year scale of IMF may be associated with changing solar activity. Specifically, an amalgamation of previous and present data showed that droughts were likely to be a historically persistent feature of the Earth's climate, whereas the probability of intensified rainfall events seemed to increase during the course of the 19th and 20th centuries. These changing characteristics in precipitation indicate an unprecedented alteration of the hydrological cycle, with unknown future amplitude. Our reconstruction complements existing information on past precipitation changes in the Qilian Mountain, and provides additional low-frequency information not previously available.

Qilian Mountain, tree-ring reconstruction, empirical mode decomposition, multi-scale precipitation variability

Citation: Tian Q H, Zhou X J, Gou X H, et al. Analysis of reconstructed annual precipitation from tree-rings for the past 500 years in the middle Qilian Mountain. Sci China Earth Sci, 2012, 55: 770–778, doi: 10.1007/s11430-012-4375-6

The Qilian Mountain lies in the northeastern Qinghai-Tibetan Plateau of northwestern China, in the interior of Euro-Asia continent. The climate of this area is influenced by the Asian Monsoon, the mid-high-latitude westerly circulation systems, and circulation above the Tibetan Plateau. This interplay of circulation systems makes the ecologic environment very fragile. In particular, changes in global

*Corresponding author (email: xjzhou@cams.cma.gov.cn)

warming and regional climate have seriously deteriorated the ecological environment in this region. The glaciers are retreating and the snow line is rising. Water resources are becoming scarcer. Thus, this area has been the focus of climate change research from an academic and practical point of view. The scarcity of weather stations and relative incompleteness of the climate records have greatly limited a more comprehensive and in-depth understanding of climate change in the region over a longtime scale. However, high-resolution tree-ring data can provide an alternative approach to overcoming this problem. Indeed, several dendroclimatological studies have been carried out in the Tibetan Plateau and have made great advances in the context of climatic reconstructions over long time scales [1–8]. Living trees with millennial longevities have been found in the Qilian Mountain since the 1970s [9], demonstrating the potential of dendrochronology in this region. In recent years, dendrochronological research has made a significant progress in this area, including reconstructions of temperature from a centennial to a millennial time scale [10–12] and reconstructions of stream flow of the Heihe River [13–15]. Moreover, the divergence phenomenon has been investigated using *Picea crassifolia* tree-rings in the upper tree line of the Qilian Mountain [16]. Drought reconstructions for the past three centuries have been built using ring width, mean early wood density and mean late wood density [17–22]. Yang et al. [23] reconstructed precipitation for the past 600 years in the western Qilian Mountain, and Zhang et al. [24, 25] reconstructed millennium-long annual precipitation. However, to the best of our knowledge, the number of precipitation reconstructions longer than 500 years is still very limited. Development of new and longer precipitation reconstructions would thus be highly advantageous for climate research. Additionally, only a few studies have focused on natural fluctuations of the reconstructed climate, and even fewer have targeted these variations of the time scale dependencies.

To address this research gap, a new tree-ring chronology with distinct paleoclimatic significance over the past five centuries was developed in the middle Qilian Mountain. The Empirical Mode Decomposition (EMD) method [26, 27] was employed to extract multi-scale variability of the reconstructed precipitation. Eight Intrinsic Mode Functions (IMFs) were extracted and used to evaluate possible dynamic links with atmospheric circulation and solar activity at different time scales. The IMFs were also used to reveal the physical mechanisms behind the precipitation fluctuations, and they may provide more comprehensive understanding of the differing time scales for intrinsic climate signals. Moreover, an amalgamation of the existing tree-ring-based precipitation proxy information provided additional paleoclimatic evidence of enhanced robustness and veracity. Compared to previous studies, our results provide insights into the internal dynamics of the climate system.

1 Precipitation reconstruction and analysis

The study area is located in the middle Qilian Mountain, which is a transitional zone between the arid and semi-arid area of western China and the humid area of eastern China. The old-growth Juniper trees preserve well between altitudes of 2600 and 3500 m a.s.l., which provided highly valuable material for dendrochronological studies. Mean annual precipitation in this area varies from 200 to 500 mm, with an uneven distribution both in space and time. Rainfall is abundant from May to August [28], and annual average temperature ranges from 0 to 5°C between 2000–3000 m a.s.l. The temperature is relatively stable, with only a subtle annual variability [29]. The mountain are perennially covered by snow at altitudes higher than 4000 m a.s.l., where modern glaciers are also found.

In September 2000, 65 cores from 32 living healthy trees of Qilian Juniper (*Juniperus przewalskii*) were collected in the middle Qilian Mountain between the altitudes of 2900 and 3150 m a.s.l. The collection site (38.78°N, 99.73°E) was situated in Sunan County of the Gansu Province (KGM2, Figure 1). The nearest meteorological station is the Sunan Station (Figure 1).

After being air dried, mounted and polished, all samples were cross-dated and measured to 0.001 mm precision and checked by COFECHA program [30]. The master series spans the period 1373–2000 (628 years). Furthermore, tree-ring width chronology was developed by the ARSTAN40 program [31] using detrending methods based mainly on negative exponential curves or straight lines of any slope. A cubic smoothing spline with a window width equal to 67% of the series length also was used in a few cases when anomalous growth trends occurred. After all these procedures, we obtained three different types of tree-ring index chronologies: Standard (STD), Residual (RES), and Arstan (ARS). In this study, we used the STD chronology (Figure 2), which preserves low-frequency signals.

Table 1 shows statistical characteristics of the KGM2 tree-ring width series. Generally, the sample size of tree-ring chronologies declines towards the early part of the chronology [32]. We used the subsample signal strength (SSS) [33] with a threshold value of 0.80 to evaluate the reliable time span of the chronology. Additionally, running average correlation (RBAR) [34] indicated that the chronology lost reliability approximately just before A.D. 1480. We ultimately used the reliable portion of the chronology back to A.D. 1480. The chronology was more reliable before A.D. 1491 (SSS>0.85).

Instrumental climate data from the Sunan Meteorological Station (Figure 1), available for the period 1957–2000 (Figure 3), was used for dendroclimatic analyses. These data show a warm, wet summer season with the highest temperature (16.28°C) and precipitation (60.97 mm) both in July. The annual mean temperature is 3.79°C, and the annual

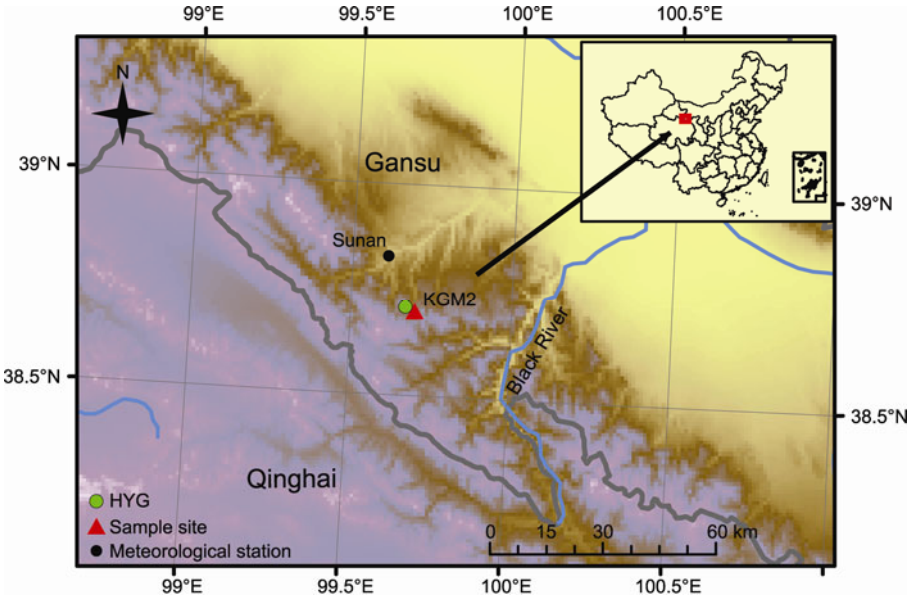

Figure 1 Map of the sampling site and meteorological station. HYG is the sampling site of Zhang et al. [24].

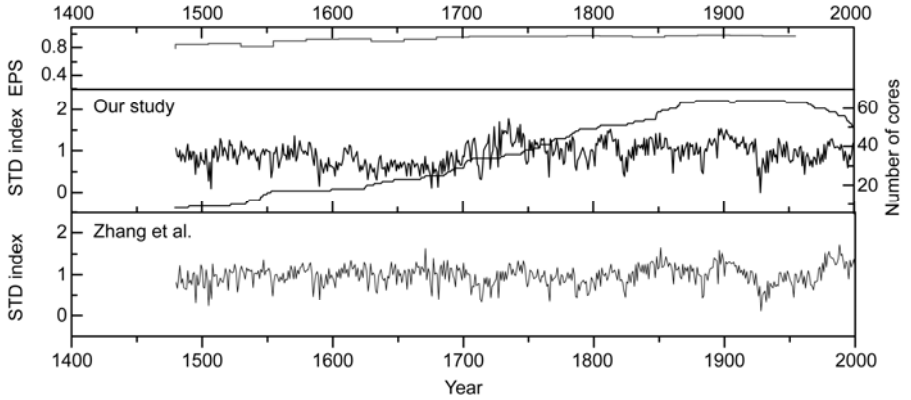

Figure 2 STD chronology, number of cores, EPS of our study and STD chronology from Zhang et al. [24].

Table 1 Statistical characteristics of the KGM2 tree-ring width series

Statistical item	KGM2
Mean sensitivity (M.S.)	0.26
Autocorrelation, the 1st order (AC1)	0.45
Mean correlations among all radii (R_1)	0.34
Mean correlations between trees (R_2)	0.33
Mean correlations within trees (R_3)	0.70
Signal-to-noise ratio (S/N)	23.69
Expressed Population Signal (EPS)	0.96
Variance, the 1st eigenvector (PC1)	38.65%
Master series coverage	1373–2000
SSS > 0.80	1468–2000
SSS > 0.85	1491–2000

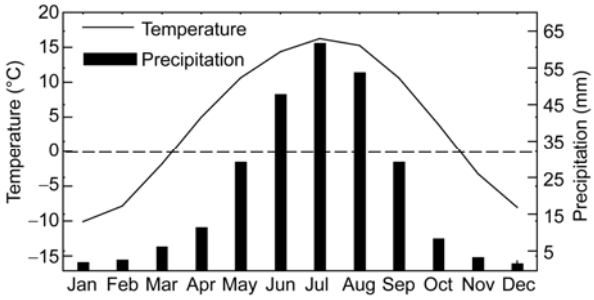

Figure 3 Monthly mean temperatures and total precipitation at the Sunan Meteorological Station.

total precipitation is 254 mm at the Sunan Station.

Correlations between tree growth and monthly temperature and precipitation data were calculated for the common period of both data series (i.e. 1957–2000), using the 14-month window approximating the growth year. Thus, the analyses included meteorological data from the prior July to the current August. As shown in Figure 4, the tree-ring width index correlated negatively with the current year temperature variables, but positively, albeit weakly, with the variables of the same parameter during the previous season (September through December) and in January, March, and

April. However, the precipitation variables of the previous year (July through September) and the current year (January through August) mainly were correlated positively with tree growth. Specifically, high correlations were found for May and June precipitation. Overall, the correlations between tree-rings and precipitation data were higher relative to temperature-correlations.

The analysis showed that precipitation is the main limiting factor for tree growth at the study area. According to the correlations, junipers produce wide annual rings during years of high precipitation in this arid and semi-arid region. During spells of elevated temperature, soil moisture loss may be caused by high rates of evapotranspiration, and these processes lead to physiological drought stress of the trees. In this condition, narrow rings are likely to be produced. Thus temperature variations could have an indirect influence on tree growth, as indicated by the observed dendroclimatic correlation pattern (Figure 4).

Among the combinations of the monthly meteorological series, the STD chronology showed the highest correlations with total precipitation of the 12-month season from previous August to the current July. The correlation was high and statistically significant (0.613, $P<0.001$). The dendroclimatic signal for the annual precipitation was an appropriate climate parameter to reconstruct from our tree-ring width chronology. Based on the above correlation analysis, we established the following transfer function:

$$P = 95.764 + 173.253\times\mathrm{STD},$$

where P represents the total precipitation of the year from the previous August to current July, and STD represents the index of the standard tree-ring chronology (KGM2).

The leave-one-out method was performed to explore the statistical fidelity of this model (Table 2). The correlation coefficient was significant at $P<0.001$ level, and the explained variance (37.6%) was strong. The results of sign tests (S1 and S2) were both significant at the 99% confidence level, reflecting a close similarity between observed and reconstructed precipitation variations. The *t*-test also passed the 99% confidence level. The positive Reduction of Error (RE) (0.33) indicated that the model had a significant reconstruction skill for the selected climate parameter (P8-7 precipitation).

Additionally, the visual comparison between the observed and reconstructed precipitation during the common period (1957–2000) was evidence that the reconstruction agreed well with the observed data (Figure 5). Combination of the results by statistical and visual comparisons demonstrates the feasibility of our data and the transfer function as a reliable paleoclimatic model for its use to reconstruct precipitation variability.

The new precipitation reconstruction indicates that climatic variability has taken place from inter-annual to longer time scales since AD 1480 (Figure 6).

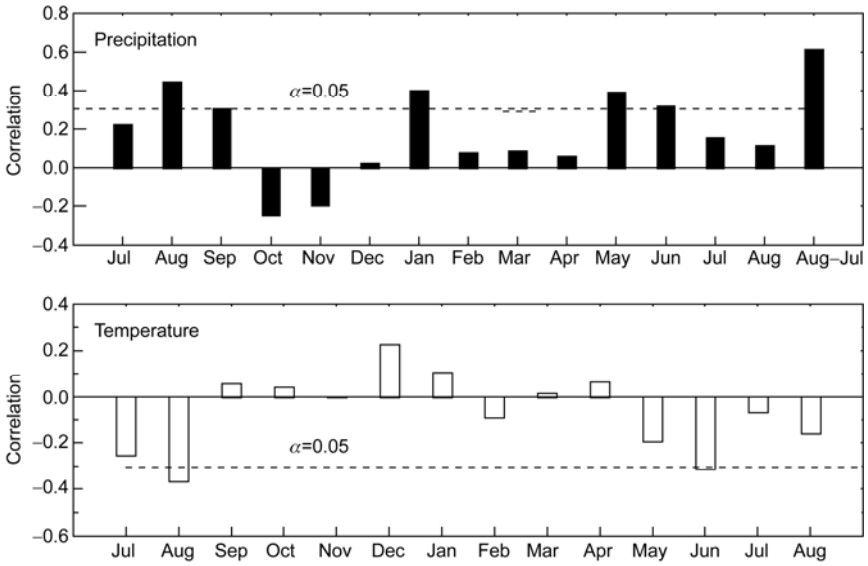

Figure 4 Correlations of tree rings with climatic data of the Sunan Station from previous July to current August. The dotted line indicates 0.05 confidence level.

Table 2 Verification statistics for the reconstruction model[a)]

R	R^2	F	S1	S2	t	RE
0.613	0.376	25.31	32 (31**, 28*)	33 (31**, 28*)	3.51 (2.71**)	0.33

a) * and ** indicate significance at the 0.05 and 0.01 level, respectively.

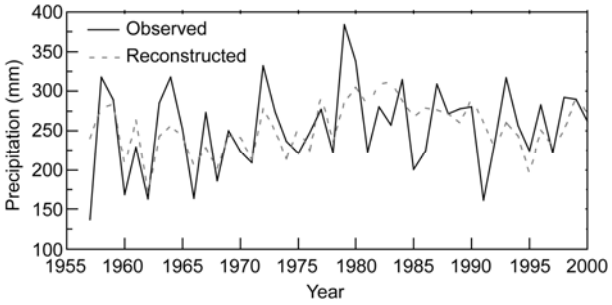

Figure 5 Observed and reconstructed annual precipitation records (1957–2000).

The mean value and standard deviation (σ) of the reconstructed series were 261.28 mm and 46.65 mm, respectively. These two statistics were used to define the precipitation extremes in the long-term context. First, we classified the "prolonged" dry intervals as the periods showing reconstructed precipitation persistently lower than the above-mentioned mean. These climatic episodes occurred during the periods 1485–1511, 1587–1607, 1619–1701, 1709–1718, 1785–1800, 1819–1831, 1878–1886, 1922–1942, 1948–1976, and 1990–1995. The prolonged wet intervals, defined as intervals showing precipitation values persistently higher than the above mentioned mean, occurred during the periods 1512– 1586, 1608–1618, 1719–1784, 1801–1818, 1832–1877, 1887–1921, 1943–1947, and 1977–1989.

In general, the 11-year running mean curve indicates a highly variable climate with alterations of drier and wetter phases prevailing through the record (Figure 6). With regard to the above-mentioned mean value, we divided the precipitation variability into four periods of "prevailing" dryness and wetness following the 11-year curve. The first such determined wet interval occurred during the first half of the 16th century (1500–1550). This was followed by a dry period during the 17th century (1600–1710), after which a period of wetness prevailed from the early 18th to 20th centuries (1720–1920). It is worth noting that this bi-centennial wet period was interrupted by an abrupt dry period during the 1920s–1930s. In addition, we defined "severe" wet periods as the intervals showing precipitation values of the 11-year curve (Figure 6) above the 1σ range (here, 307.93 mm), and "severe dry periods" as the intervals below the 1σ range (here, 214.63 mm). Using these criteria, we found that three severe wet periods had occurred during the periods 1728–1743, 1808–1812, and 1896–1907, as well as two severe dry periods during the periods 1670–1685 and 1928–1933. The severe drought of the early 20th century (during 1920s–1930s) has been reported in several previous studies [35, 36] as an extreme climatic event typified by consecutive dry years in China over large spatial scales.

We note that our reconstruction was highly correlative with the tree-ring-based annual precipitation variability, as reconstructed by Zhang et al. [25]. The correlation coefficient between the two reconstructions was 0.627, as calculated over the common period (1480–2000). The high correlativity between the two series further confirmed the reliability of the record of paleoclimate variability at the studied sites in the Qilian Mountain. Interestingly, the two reconstructions somewhat disagreed during the 17th century when the new reconstruction demonstrated more severe drought. These results underscore the need for spatially more detailed tree-ring data to better retrieve and understand past and present patterns of regional climatic variation.

2 EMD analysis of precipitation reconstruction at multi-scales

The empirical mode decomposition method (EMD) was first proposed by Huang et al. [26] in 1998. It is a new technique to comprehensively analyze various types of data, and especially used to understand multi-scale patterns of data behavior. The EMD has the advantage that it can be used to efficiently extract information in both time and frequency domains directly from the integrated variations and trends. The method has been widely applied in many scientific fields, such as signal and image processing, as well as in atmospheric science [37–39]. Here, we employed the EMD method to more comprehensively understand the obtained precipitation variations over the past 521 years on multiple

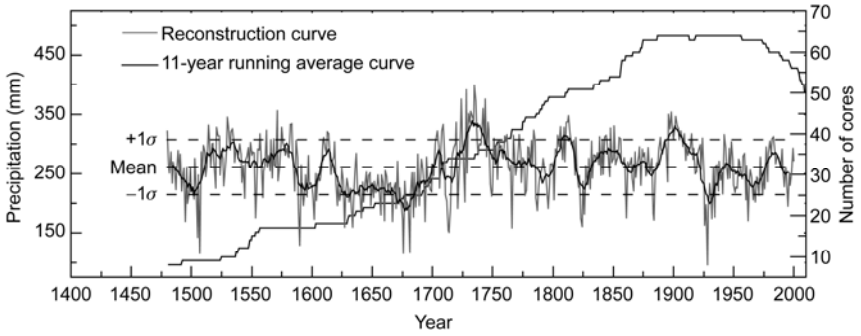

Figure 6 Precipitation reconstruction for the Middle Qilian Mountain from AD 1480 to 2000 with its 11-year running mean curve. The range of standard deviation (σ) indicates long-term anomaly boundaries.

time scales.

In essence, the signal is decomposed into a class of intrinsic mode functions (IMFs). These modes of oscillation are the components that retain features of natural oscillations in the overall signal, independent of one another. By integrating all IMFs and the residue, the original signal is recovered. Importantly, the IMF components might be attributable to certain physical processes, known to bear similar modes of oscillations as the IMF of the analyzed data. The residue represents the trend in the data, showing the lowest frequency of available variations with a period longer than the length of the data. A detailed introduction of the method was given by Huang et al. [26].

The EMD analysis found eight IMFs, extracted from the precipitation reconstruction, showing the instantaneous variation of the determined frequencies and their corresponding precipitation amplitudes on a relatively narrow band (Figure 7).

The IMF components show nonlinear variations of natural climatic signals on multiple time scales of their specific quasi-period (also called "major period"). However, the original (integrated) precipitation variations, and the importance and influence of the different IMFs vary considerably. The signal intensity and energy can be evaluated by the square of the IMF's amplitude, whereas the correlation coefficient can be used to indicate the weight of the IMF with regard to the original data (Table 3).

The IMF1 and IMF4 components had the highest correlations with the original data, and these two IMFs also showed large amplitudes. These features indicate that these two IMFs could represent large portions of the original precipitation variability. The IMF2 and IMF3 components performed with moderate correlations and considerable amplitudes. The correlations of IMF5 and IMF6 with the original reconstructed precipitation were already lower than 0.3. Nevertheless, the fluctuations in IMF6 showed marked changes around AD 1800, indicating that this function was characterized additionally by time-dependent behavior. The IMF7 and IMF8 components represented precipitation variations on multi-centennial scales. However, correlations with precipitation reconstruction lower than 0.2 revealed concomitant diminishments in their amplitudes. These results indicate reduced signal intensity relative to the total variability of the reconstruction. In the following section, the frequency and amplitude of each of the IMFs are used to discuss the main characteristics of the precipitation varia-

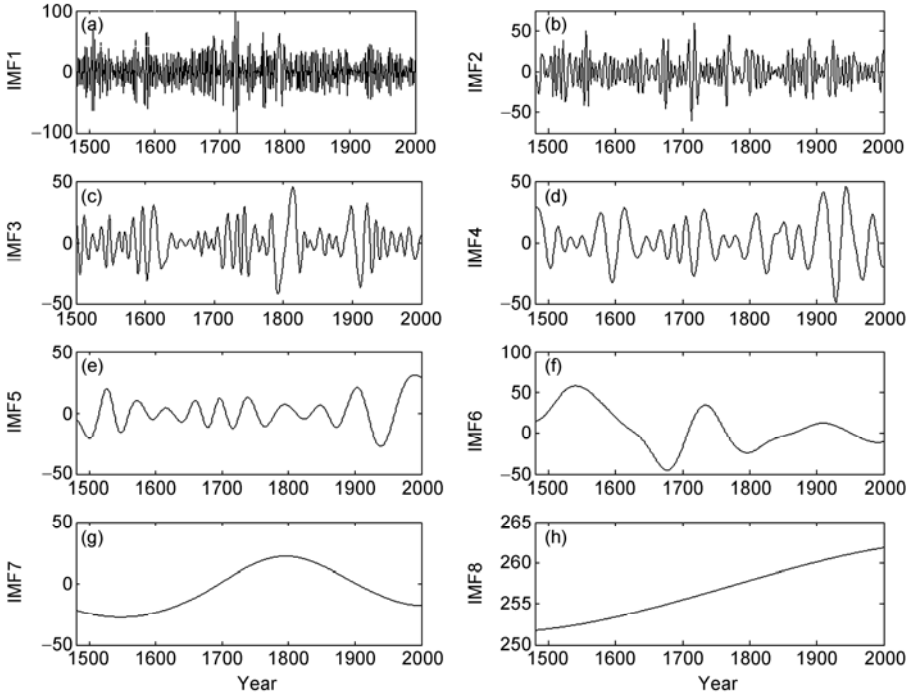

Figure 7 IMF components of the precipitation data.

Table 3 Statistics of the IMF components

IMF	IMF1	IMF2	IMF3	IMF4	IMF5	IMF6	IMF7	IMF8
Major cycles	2–3	5–8	10–13	29	50–64			
Max. amplitude	110	60	45	45	30	60	25	
Correlation coefficient	0.52	0.34	0.35	0.43	0.27	0.29	0.16	0.07

tions on different time scales.

3 Discussion of precipitation multi-scale variability

The EMD analysis divided the original precipitation reconstruction into multiple time scales. The extracted components of the precipitation variability revealed the temporal distribution and detailed fluctuations of the major periods by their corresponding amplitudes in the time-frequency domain.

The major period of the IMF1 was 2–3 years (Figure 7(a)). The period was relatively stable in the time-frequency domain. The IMF1 had the strongest signal, representing a major portion of the high-frequency variations in the reconstructed precipitation. Conceivably the IMF1 may be associated with the quasi-biennial oscillation (QBO) and quasi-triennial oscillation (QTO) [40, 41]. This suggests that the IMF1 results from periodic shifts between easterly and westerly winds in the stratosphere of the equatorial region, with highly similar quasi-oscillation of 2–3 year periodicity. The maximum amplitude observed in the IMF1 occurred around the 1720s, coeval with the reconstructed wetness. Conversely the lowest amplitude occurred during the 1920s, corresponding to an anomalously dry period at that time. The major period of the IMF2 was 5–8 years (Figure 7(b)), and may be associated with an atmospheric oscillation closely connected to the frequently documented variations in the ENSO [42].

The IMF3 component displayed precipitation variations on a 10–13 year timescale (Figure 7(c)). The similarity of the IMF3 timescale and the 11-year cycle of sunspots [43] may indicate a relationship between precipitation and solar activity for the study region. Moreover, there were several sudden changes in the frequency and amplitude of the IMF3 in its time domain. In particular, the amplitude and signal intensity abruptly weakened during the dry interval of 1620–1710, when it was slightly dry. Two other abrupt changes of the IMF3 occurred during the early 19th and early 20th centuries, when the major period metamorphosed into a longer cycle of 27 years. However, the amplitude of this variation was rapidly weakened in the course of the 19th century, as compared to the change in the early 20th century, when its amplitude was much greater. The IMF4 component mainly represented inter-decadal variations in the reconstructed precipitation approximating the periodicity at a 29 year timescale, of which cycle length and amplitude varied only a minor amount (Figure 7(d)).

The IMF5 component showed a relatively stable oscillation on a 50–64 year timescale. However, larger fluctuations are seen at the beginning and end part of the reconstruction (Figure 7(e)). The IMF6 component revealed the potential for an unstable oscillation of the drought and rainfall on a centennial scale (Figure 7(f)), with its three wave peaks corresponding to high precipitation during the 1540s, 1740s, and 1900s. Conversely the large wave trough of the 1680s corresponded to a relatively dry phase in our reconstruction. Likewise, precipitation fluctuation of this type has clearly weakened since the 19th century. The IMF7 component showed a relatively weak but profoundly proceeding wave as an essential part of the total precipitation oscillation over the past five centuries (Figure 7(g)). The peak of this wave fell on the metaphase with the persistent wet period (from the 18th to the beginning of the 20th century), indicating an occurrence of a dry-wet-dry low-frequency cycle in the Qilian Mountain. However, the small amplitude and low correlation with the initial reconstruction suggests that this centennial signal has only a low explanatory power.

The IMF8 component was the last residue after all the IMFs were extracted from our precipitation reconstruction (also termed "Residue"). Its amplitude ranged from a reconstructed precipitation amount of 252 to 262 mm, totaling about 10 mm. Moreover, the IMF8 indicates a slowly increasing trend over the past 521 years (Figure 7(h)). Due to the limitation of data length in our study, it could not be ascertained whether the IMF8 is a part of a climatic cycle of longer duration or an aperiodic nonlinear trend.

4 A proxy-amalgamation

A comparison of previously published precipitation reconstruction signals [23, 25] with our data provides paleoclimatic information with increased veracity. Using an approach superimposing available paleoclimatic evidence, the data of anomalous droughts and rainfall periods were amalgamated (Figure 8). Only the periods with all three reconstructions showing synchronous precipitation anomalies were accepted as the most reliable indications of such events. As shown by the horizontal bars, it was found that the reconstructions indicated three distinct events of past droughts: 1486–1489, 1713–1715, and 1928–1932. These events were temporally spread over the past six centuries. By contrast, the events of intensified rainfall occurred only during the recent past (Figure 8). These were periods of wetness occurring during 1843–1845, 1854–856, 1892–1894, 1896–1899, 1901–1907, and 1980–1985.

Amalgamation of the data indicates that droughts have likely been a more or less persistent feature in the Qilian Mountain through the centuries. On the other hand, intensified rainfall events appeared to have increased toward the present-day, during the course of the 19th and 20th centuries. It is notable that our reconstruction indicated a long-term rise of precipitation levels (Figure 7(h)). This finding is broadly consistent with results from a previous study that indicated intensified pluvial conditions during the 20th century in the Heihe River Basin [14], and from indications of coinciding wetness by other research [44, 45]. The changing characteristics of precipitation variability imply that the

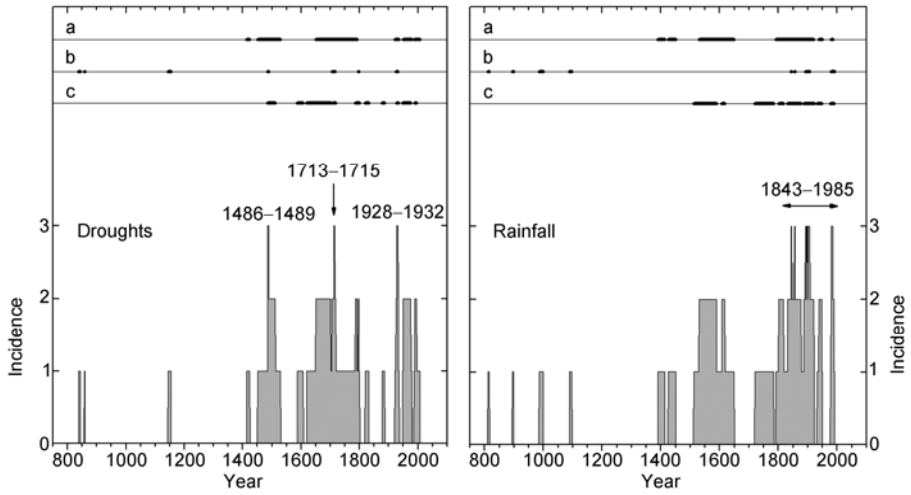

Figure 8 Amalgamation of precipitation information. The horizontal lines were the reconstructed droughts and rainfall events by Yang et al. [23] (a), Zhang et al. [25] (b) and our results (c). The vertical bars were the incidence of the overlapping evidence counted of the reconstructed droughts and rainfall events by Yang et al. [23], Zhang et al. [25] and our results.

hydrological cycle may have undergone unprecedented alterations. Previous explanations have considered that the 20th century wetness anomaly could relate to global warming [46]. The amplitude of forthcoming hydrological events is unknown. However, the increasing amount of information of past precipitation conditions may improve our understanding of the ongoing change. Thus, our results underscore the need for a greater number of long tree-ring based precipitation records for the region.

5 Conclusions

A new moisture-sensitive tree-ring width chronology of Qilian Juniper was constructed for the middle Qilian Mountain. Consequently the annual precipitation (from previous August to current July) was reconstructed over the past 521 years. This study provides a new long-term hydrometeorological series for regional climate analysis. The chronology and reconstruction both serve as important supplements for the regional tree-ring network and for reconstructions of spatial fields of the past climate.

The reconstructed precipitation of this study showed four distinct alterations of dry and wet spells over the past five centuries. Using the EMD method, eight IMF components originally embedded in the reconstruction were extracted, which represented climate oscillations at high- to low-frequencies. The IMF components of 2–3 and 5–8 year timescales were captured as the main variations of the initial precipitation data, revealing that precipitation variability in the middle Qilian Mountain could be influenced by ocean-atmosphere circulations, such as the QBO/QTO phenomena and the ENSO, respectively. The IMF components representing climate variations on timescales of 10–13 years were found to mimic variations of similar characteristics in solar activity. The amalgamation of three studies indicates that intensified rainfall events in the past two centuries agree with the slowly increasing trend of precipitation shown by the IMF8 component.

This work is a pioneering effort to explore variability in tree-ring-based precipitation reconstructions on multiple scales using the EMD method. Compared with traditional tree-ring research, we provide physically more meaningful interpretations of the possible underlying dynamic processes than previous studies. Overall, the study emphasizes the great potential of the employed methodologies for analysis of the multi-scale variability and dynamics of past and ongoing climate changes. Moreover, the amalgamation provides more reliable precipitation information.

This work was supported by the National Natural Science Foundation of China (Grant Nos. 41001058, 41001009, 40971119 and 40890052), the China Postdoctoral Science Foundation (Grant Nos. 201003194). We thank Dr. Zhang F, Dr. Zhu C S and Dr. Zhang Y for their assistance with this study. We also thank two reviewers for their invaluable suggestions.

1 Shao X M, Huang L, Liu H B, et al. Reconstruction of precipitation variation from tree rings in recent 1000 years in Delingha, Qinghai. Sci China Ser D-Earth Sci, 2005, 48: 939–949
2 Shao X M, Xu Y, Yin Z Y, et al. Climatic implications of a 3585-year tree-ring width chronology from the northeastern Qinghai-Tibetan Plateau. Quat Sci Rev, 2010, 29: 2111–2122
3 Liu Y, An Z S, Ma H Z, et al. Precipitation variation in the northeastern Tibetan Plateau recorded by the tree rings since 850 AD and its relevance to the Northern Hemisphere temperature. Sci China Ser D-Earth Sci, 2006, 49: 408–420
4 Liu Y, An Z S, Han W L, et al. Annual temperatures during the last 2485 years in the mid-eastern Tibetan Plateau inferred from tree rings. Sci China Ser D-Earth Sci, 2009, 52: 348–359
5 Zhang Q B, Guo D C, Tan D Y, et al. A 2326-year tree-ring record of climate variability on the northeastern Qinghai-Tibetan Plateau. Geophys Res Lett, 2003, 30: 1739–1742
6 Sheppard P R, Tarasov P E, Graumlich L J, et al. Annual precipita-

tion since 515 BC reconstructed from living and fossil juniper growth of northeastern Qinghai Province, China. Clim Dyn, 2004, 23: 869–881
7 Gou X H, Deng Y, Chen F H, et al. Tree ring based streamflow reconstruction for the upper Yellow River over the past 1234 years. Chin Sci Bull, 2010, 55: 3236–3243
8 Kang X C, Zhang Q H, Graumlich L J, et al. Reconstruction of A 1835 a past climate for Dulan, Qinghai Province, using tree ring (in Chinese). J Glaciol Geocryol, 2000, 22: 65–72
9 Wang Y X, Liu G Y, Zhang X G, et al. The relationship between the tree ring of *Sabina przewalskii* and climate changes of thousand years, glacier activity in Qilian Mountain. Chin Sci Bull, 1982, 27: 1316–1319
10 Liu X H, Qin D H, Shao X M, et al. Temperature variations recovered from tree-rings in the middle Qilian Mountain over the last millennium. Sci China Ser D-Earth Sci, 2005, 48: 521–529
11 Liu X H, Shao X M, Zhao L J, et al. Dendroclimatic temperature record derived from tree-ring width and stable carbon isotope chronologies in the Qilian Mountain, China. Arct Antarct Alp Res, 2007, 39: 651–657
12 Tian Q H, Gou X H, Zhang Y, et al. May–June temperature reconstruction over the past 300 years based on tree rings on the Qilian Mountain of Northeastern Tibetan. IAWA J, 2009, 30: 421–434
13 Liu Y, Sun J Y, Song H M, et al. Tree-ring hydrologic reconstructions for the Heihe River watershed, western China since AD 1430. Water Res, 2010, 44: 2781–2792
14 Qin C, Yang B, Burchardt I, et al. Intensified pluvial conditions during the twentieth century in the inland Heihe River Basin in arid northwestern China over the past millennium. Glob Planet Change, 2010, 72: 192–200
15 Kang X C, Cheng G D, Kang E S, et al. Mountain outlet runoff reconstruction of the Heihe River during past 1000 years using tree rings. Sci China Ser D-Earth Sci, 2002, 32: 675–685
16 Zhang Y X, Shao X M, Wilmking M. Dynamic relationships between *Picea crassifolia* growth and climate at upper treeline in the Qinlian Mts., Northeast Tibetan Plateau, China. Dendrochronologia, 2011, 29: 185–199
17 Chen F, Yuan Y, Wei W. Climatic response of *Picea crassifolia* tree-ring parameters and precipitation reconstruction in the western Qilian Mountain, China. J Arid Environ, 2011, 75: 1121–1128
18 Tian Q H, Gou X H, Zhang Y, et al. Tree-ring based drought reconstruction (A.D. 1855–2001) for the Qilian Mountain, northwestern China. Tree-ring Res, 2007, 63: 27–36
19 Gou X H, Chen F H, Wang Y J, et al. Spring precipitation reconstructed in the east of the Qilian Mountain during the last 280 a by tree ring width (in Chinese). J Glaciol Geocryol, 2001, 23: 292–296
20 Wang Y J, Chen F H, Gou X H. Reconstruction of spring precipitation in the middle region of the Qilian Mountain using tree-ring data (in Chinese). Sci Geogr Sin, 2001, 21: 373–377
21 Liang E Y, Shao X M, Liu X H. Annual precipitation variation inferred from tree rings since AD 1770 for the western Qilian Mts., northern Tibetan Plateau. Tree Ring Res, 2009, 65: 95–103
22 Liu W H, Gou X H, Yang M X, et al. Drought reconstruction in the Qilian Mountain over the last two centuries and its implications for large-scale moisture patterns. Adv Atmos Sci, 2009, 26: 621–629
23 Yang B, Qin C, Bräuning A, et al. Rainfall history for the Hexi Corridor in the arid northwest China during the past 620 years derived from tree rings. Int J Climatol, 2011, 31: 1166–1176
24 Zhang Y, Gou X H, Chen F H, et al. A 1232 years tree-ring record of climate variability in the Qilian Mountain, Northwestern China. IAWA J, 2009, 30: 407–420
25 Zhang Y, Tian Q H, Gou X H, et al. Annual precipitation reconstruction since A.D. 775 based on tree rings from the Qilian Mountain, northwestern China. Int J Climatol, 2011, 31: 371–381
26 Huang N E, Shen Z, Long S R, et al. The empirical mode decomposition method and the Hilbert spectrum for non-stationary time series analysis. Proc Roy Soc London, 1998, 454A: 903–995
27 Huang N E, Shen Z, Long S R. A new view of nonlinear water waves-the Hilbert spectrum, Ann Rev Fluid Mech, 1999, 31: 417–457
28 Yang Q, Liu J, Wang Y. Survey Report in the National Nature Reserve of Qilian Mountain, Gansu (in Chinese). Lanzhou: Gansu Science & Technology Press, 2008
29 Zhang C J, Guo N. Climatic variation characteristics over Qilian Mountain area during the last 40 years (in Chinese). Meteorology, 2002, 28: 33–39
30 Stokes M A, Smiley T L. An Introduction to Tree Ring Dating. Chicago: The University of Chicago Press, 1968
31 Cook E R. A time-series analysis approach to tree-ring standardization. Dissertation for the Doctoral Degree. Tucson: University of Arizona, 1985
32 Fritts H C. Tree Rings and Climate. London: Academic Press, 1976
33 Wigley T M L, Briffa K R, Jones P D. On the average value of correlated time series, with applications in dendroclimatology and hydrometeorology. J Clim Appl Meteorol, 1984, 23: 201–213
34 Briffa K R. Interpreting high-resolution proxy climate data-the example of dendroclimatology. In: von Storch H, Navarra A, eds. Analysis of Climate Variability, Applications of Statistical Techniques. Berlin Heidelberg New York: Springer, 1995. 77–94
35 Liang E Y, Liu X H, Yuan Y J, et al. The 1920s drought recorded by tree rings and historical documents in the semiarid areas of Northern China. Clim Change, 2006, 79: 403–432
36 Li J, Chen F, Cook E R, et al. Drought reconstruction for north central China from tree rings: The value of the Palmer Drought Severity Index. Int J Climatol, 2007, 27: 903–909
37 Yang P C, Wang G L, Bian J C, et al. The prediction of non-stationary climate series based on empirical mode decomposition. Adv Atmos Sci, 2010, 27: 845–854
38 Deng Y J, Wang W, Qian C C, et al. Boundary-processing-technique in EMD method and Hibert transform. Chin Sci Bull, 2001, 46: 1–8
39 Lin Z S, Wang S G. EMD analysis of northern hemisphere temperature variability during last 4 centuries (in Chinese). J Tropi Meteorol, 2004, 20: 90–96
40 Gordon A H, Byron-Scott R A, Bye J A. A note on QBO-SO interaction, the quasi-triennial oscillation and the sunspot cycle. J Atmos Sci, 1982, 39: 2083–2087
41 Naujokat B. An update of the observed Quasi-Biennial Oscillation of stratospheric winds over the tropics. J Atmos Sci, 1986, 43: 1873–1877
42 Allan R, Lindesay J, Parker D. El Nino, Southern Oscillation and Climatic Variability. Commonwealth Scientific and Industrial Research Organization. Melbourne: Australia Press, 1996
43 Prabhakaran Nayar S R, Radhika V N, Revathy K, et al. Wavelet analysis of solar wind and geomagnetic parameters. Solar Phys, 2002, 208: 359–373
44 Ma X B, Shi Y F, Shen Y P, et al. An analysis of climate changing trend in Northwest China: Recent and historical periods. J Glaciol Geocryol, 2003, 25: 672–675
45 Shi Y F, Shen Y P, Hu R J. Preliminary study on signal, impact and foreground of climatic shift from warm-dry to warm-humid in Northwest China. J Glaciol Geocryol, 2002, 24: 199–225
46 Treydte K S, Schleser G H, Helle G, et al. The twentieth century was the wettest period in northern Pakistan over the past millennium. Nature, 2006, 440: 1179–1182